(*E. coli*), which is essential for proton transport (*20*).

Our results indicate that the c subunit oligomer rotates with the γ subunit during ATP hydrolysis by $F_0F_1$. In the reverse direction, proton transport should drive rotation of the c subunit oligomer, which in turn would drive rotation of the γ subunit to promote ATP synthesis. Our study demonstrates that the mechanical rotation of the γ and c subunit complex is an essential feature for the energy coupling between proton transport through the $F_0$ sector and ATP hydrolysis or synthesis in the $F_1$ sector. Analysis of a series of *E. coli* $F_0F_1$ mutants (*21*), based on the progress of single molecule biomechanics (*22*), will contribute to the further understanding of the motor mechanism.

### References and Notes


1. M. Futai, T. Noumi, M. Maeda, *Annu. Rev. Biochem.* **58**, 111 (1989); M. Futai and H. Omote, in *Handbook of Biological Physics, Volume 2*, W. N. Konings, H. R. Kaback, J. S. Lolkema, Eds. (Elsevier, Amsterdam, 1996), pp. 47–74; J. Weber and A. E. Senior, *Biochim. Biophys. Acta* **1319**, 19 (1997); R. H. Fillingame, *Curr. Opin. Struct. Biol.* **6**, 491 (1996); H. S. Penefsky and R. L. Cross, *Adv. Enzymol. Relat. Areas Mol. Biol.* **64**, 173 (1991).
2. P. D. Boyer, *Annu. Rev. Biochem.* **66**, 717 (1997).
3. J. P. Abrahams, A. G. W. Leslie, R. Lutter, J. E. Walker, *Nature* **370**, 621 (1994).
4. H. Wang and G. Oster, *Nature* **396**, 279 (1998).
5. R. Aggeler, M. A. Haughton, R. A. Capaldi, *J. Biol. Chem.* **270**, 9185 (1995); T. M. Duncan, V. V. Bulygin, Y. Zhou, M. L. Hutcheon, R. L. Cross, *Proc. Natl. Acad. Sci. U.S.A.* **92**, 10964 (1995).
6. H. Noji, R. Yasuda, M. Yoshida, K. Kinoshita Jr., *Nature* **386**, 299 (1997).
7. H. Omote *et al.*, *Proc. Natl. Acad. Sci. U.S.A.* **96**, 7780 (1999).
8. S. B. Vik and B. J. Antonio, *J. Biol. Chem.* **269**, 30364 (1994); W. Junge, H. Lill, S. Engelbrecht, *Trends Biochem. Sci.* **22**, 420 (1997); T. Elston, H. Wang, G. Oster, *Nature* **391**, 510 (1998); P. Dimroth, H. Wang, M. Grabe, G. Oster, *Proc. Natl. Acad. Sci. U.S.A.* **96**, 4924 (1999).
9. Y. Kato-Yamada, H. Noji, R. Yasuda, K. Kinoshita Jr., M. Yoshida, *J. Biol. Chem.* **273**, 19375 (1998).
10. The engineered *E. coli* $F_0F_1$ (αHis tag/cGlu$^2$ → Cys$^2$/γCys$^{87}$ → Ala$^{87}$/γCys$^{112}$ → Ala$^{112}$) was purified as described (*23*). The enzyme was treated with 100 μM 6-{*N*′-[2-(*N*-maleimido)ethyl]-*N*-piperazinylamido} hexyl D-biotinamide (Dojindo, Kumamoto, Japan) for 1 hour at 4°C. Specific biotinylation of the c subunit was confirmed by protein immunoblotting with streptavidin conjugated with alkaline phosphatase (Novagen, Madison, WI). This engineered $F_0F_1$ was used for rotation assay throughout our study. Fluorescently labeled biotinylated actin filaments were prepared as described (*7*). We also tested an engineered $F_0F_1$ (cGlu$^2$ → Cys$^2$) fused with biotin binding protein at the $NH_2$-terminus of the α subunit to bind the streptavidin-actin complex. The $F_0F_1$ was fixed through c subunit Cys$^2$ on beads coated with *N*-succinimidyl 4-maleimidobutyrate (Dojindo). This system produced no rotating filament.
11. Two cysteine residues (Cys$^{87}$ and Cys$^{112}$) present in the γ subunit were replaced by site-directed mutagenesis that was based on polymerase chain reaction (*7*).
12. Y. Sambongi *et al.*, data not shown.
13. The engineered enzyme was immobilized by the slightly modified method previously described (*7*). Buffer A was included in all solutions used, unless otherwise specified, and was composed of the following: 10 mM Hepes-NaOH (pH 7.8), 25 mM KCl, 6 mM $MgCl_2$, bovine serum albumin (BSA) (10 mg/ml), and 0.24 mM Triton X-100. Ni–nitrilotriacetic acid horseradish peroxidase conjugate (0.8 μM) (Qiagen, Valencia, CA) in buffer A (without BSA and Triton X-100), 10 nM $F_0F_1$, and 4 μM streptavidin were successively introduced into the flow cell. Fluorescently labeled actin filaments (12.5 nM) were added to construct $F_0F_1$ with an attached actin filament, and finally, the reaction mixture for rotation [5 mM Mg ATP, 1 μM biotin, pyruvate kinase (50 μg/ml), 1 mM phosphoenol pyruvate, 25 mM glucose, 1% β-mercaptoethanol, glucose oxidase (216 μg/ml), and catalase (36 μg/ml) in buffer A] was introduced. The rotation was observed at 20°C with a Zeiss Axiovert 135 equipped with an intensified charge-coupled device camera (Atto Instruments, Rockville, MD) and was video recorded. The rotation angle of the filament was estimated from the centroid of the actin filament.
14. Immediately after the ATP addition, we rapidly scanned the 0.5-mm$^2$ area of a flow cell (containing <250 filaments) for 2 min. Under the standard assay conditions (*13*), we found at least one rotating filament in the cell. The following observations show that the rotating filaments were those connected to the c subunit: (i) The c subunit rotation could be observed in the presence of Triton X-100 but not in the absence of the detergent (0 rotating filaments out of 12,000). The addition of detergent may imitate the native lipid environment. In contrast, the γ subunit rotation in engineered $F_1$ was not dependent on the presence of the detergent. (ii) We isolated $F_1$ (no cysteine in the γ subunit, cysteine-less γ) from $F_0F_1$ (engineered for c subunit rotation) to test whether the actin filament can bind to the cysteine-less γ and rotate after the addition of ATP. We could find no rotating filaments (out of 10,000 filaments), which indicated that the contaminating $F_1$ (with cysteine-less γ), if any, is not responsible for the present results. (iii) SDS-polyacrylamide gel electrophoresis of the engineered $F_0F_1$ gave the same subunit ratio as that of previous reported preparations (*23*), indicating that the contamination of $F_1$ is minor. The rotation frequency of the filament directly connected to the $F_1$ γ subunit was slightly higher; about three filaments were observed when we rapidly scanned the area of ~0.5 mm$^2$ as described above.
15. Real-time video images of rotating filaments connected to the c subunit are available at www.sciencemag.org/feature/data/1045705.shl
16. P. C. Jones, W. Jiang, R. H. Fillingame, *J. Biol. Chem.* **273**, 17178 (1998); P. C. Jones and R. H. Fillingame, *J. Biol. Chem.* **273**, 29701 (1998); O. Y. Dmitriev, P. C. Jones, R. H. Fillingame, *Proc. Natl. Acad. Sci. U.S.A.* **96**, 7785 (1999).
17. D. S. Perlin, L. R. Latchney, A. E. Senior, *Biochim. Biophys. Acta* **807**, 238 (1985).
18. A pause was defined from the median filtered linear segment (as shown in Fig. 3A) as having coefficient of determination $R^2$ values of >0.96, a rotational rate between −0.2 and 0.2 rotations per second, and a dwell time of >67 ms.
19. We titrated the effects of venturicidin concentrations on the c subunit rotation and showing the results from 7 and 70 μM (Fig. 3B). The higher concentration was necessary for the inhibition under the rotation conditions. When we tested the effects of venturicidin in buffer A (*13*) containing 5 mM Mg ATP, 1 μM biotin, pyruvate kinase (50 μg/ml), 1 mM phosphoenol pyruvate, 25 mM glucose, 1% β-mercaptoethanol, glucose oxidase (216 μg/ml), and catalase (36 μg/ml), the inhibition of ATPase activity of $F_0F_1$ (purified or membranes) was ~10-fold lower than that reported previously (*20*). The weaker inhibitory effect was possibly due to the chemicals included in this study. The antibiotic was not inhibitory to the ATPase activity of $F_1$ under the same conditions.
20. R. H. Fillingame, M. Oldenburg, D. Fraga, *J. Biol. Chem.* **266**, 20934 (1991).
21. A. Iwamoto, J. Miki, M. Maeda, M. Futai, *J. Biol. Chem.* **265**, 5043 (1990); K. Shin, R. K. Nakamoto, M. Maeda, M. Futai, *J. Biol. Chem.* **267**, 20835 (1992); R. K. Nakamoto, M. Maeda, M. Futai; *J. Biol. Chem.* **268**, 867 (1993); R. K. Nakamoto, M. K. Al-Shawi, M. Futai, *J. Biol. Chem.* **270**, 14042 (1995); M. K. Al-Shawi, C. J. Ketchum, R. K. Nakamoto, *J. Biol. Chem.* **272**, 2300 (1997); C. Jeanteur–de Beukelar, H. Omote, A. Iwamoto-Kihara, M. Maeda, M. Futai, *J. Biol. Chem.* **270**, 22850 (1995).
22. A. D. Mehta, M. Rief, J. A. Spudich, D. A. Smith, R. M. Simmons, *Science* **283**, 1689 (1999).
23. Y. Moriyama, A. Iwamoto, H. Hanada, M. Maeda, M. Futai, *J. Biol. Chem.* **266**, 22141 (1991).
24. R. Yasuda, H. Noji, K. Kinoshita Jr., M. Yoshida, *Cell* **93**, 1117 (1998); A. J. Hunt, F. Gittes, J. Howard, *Biophys. J.* **67**, 766 (1994).
25. K. Svoboda, C. F. Schmidt, B. J. Schnapp, S. M. Block, *Nature* **365**, 721 (1993).


26. Supported in part by the Japanese Ministry of Education, Science, and Culture and by the Naito Foundation. We thank K. Saito and R. H. Fillingame for helpful discussions, M. A. Spies for critical reading of the manuscript, and N. Sambonmatsu for her technical assistance.

24 September 1999; accepted 28 October 1999


# Visualization of Dioxygen Bound to Copper During Enzyme Catalysis


**C. M. Wilmot,[1] J. Hajdu,[2] M. J. McPherson,[1] P. F. Knowles,[1] S. E. V. Phillips[1]**



X-ray crystal structures of three species related to the oxidative half of the reaction of the copper-containing quinoprotein amine oxidase from *Escherichia coli* have been determined. Crystals were freeze-trapped either anaerobically or aerobically after exposure to substrate, and structures were determined to resolutions between 2.1 and 2.4 angstroms. The oxidation state of the quinone cofactor was investigated by single-crystal spectrophotometry. The structures reveal the site of bound dioxygen and the proton transfer pathways involved in oxygen reduction. The quinone cofactor is regenerated from the iminoquinone intermediate by hydrolysis involving Asp$^{383}$, the catalytic base in the reductive half-reaction. Product aldehyde inhibits the hydrolysis, making release of product the rate-determining step of the reaction in the crystal.


Oxygen is a ubiquitous electron acceptor in aerobic biological systems. The mechanisms of oxygen activation by redox enzymes, including *Escherichia coli* amine oxidase (ECAO), are poorly understood. To address this, we have used flash-freezing techniques on catalytically competent crystals of ECAO to trap intermediates in the oxidative half-reaction, and solve the

structures by single-crystal x-ray crystallography. ECAO is representative of copper-containing amine oxidases (CuAOs), homodimeric enzymes ranging in size from 140 to 180 kD (*1*). Each subunit contains a single copper ion and a quinone cofactor, 2,4,5-trihydroxyphenylalanine quinone (TPQ) at the active site (*2*). TPQ is generated from an intrinsic tyrosine in the amino acid sequence by a self-processing event that requires only the bound copper ion and molecular oxygen (*3*).

The structure of ECAO has been determined crystallographically to 2.0 Å (Fig. 1) (*4, 5*), and the crystal structures for pea seedling CuAO (*6*), *Arthrobacter globiformis* CuAO (*7*), and *Hansenula polymorpha* CuAO (*8*) are also known. In ECAO, each subunit consists of four distinct domains: an $NH_2$-terminal domain (D1, ~90 amino acids), which is not present in all CuAOs; two homologous and conserved domains (D2 and D3, ~100 amino acids each), which have a cystatin-like fold; and a large β-sandwich domain (D4, ~440 amino acids), which contains the active site. D3 and D4 form the substrate amine entry channel and the back of the substrate-binding pocket (*7–9*). The central water-filled cavity of the dimer interface is proposed to be the entry site for molecular oxygen (*8*). The copper is coordinated in an approximately square pyramidal arrangement by three conserved His residues ($His^{524}$, $His^{526}$, and $His^{689}$) and two water molecules—one axial to the $Cu^{2+}$ (Wa) and the other equatorial (We) (Fig. 1B). The TPQ is close to, but not directly liganded to, the $Cu^{2+}$ and appears to have high rotational mobility in ECAO, the major conformation involving a hydrogen bond between O-2 of TPQ and the axial water ligand of the copper ion. TPQ O-4 is hydrogen-bonded to the hydroxyl group of conserved $Tyr^{369}$, and TPQ O-5 points into the substrate-binding pocket lying close to the conserved $Asp^{383}$, the catalytic base in the reductive half-reaction (*9*).

The catalytic reaction of the enzyme divides into two half-reactions: a reductive half and an oxidative half (Fig. 2A) (*10*). Crystallographic (*9*) and solution studies (*1*) have shown that the enzyme is reduced through dissociation of a Schiff base from the 5 position of the quinone. This part of the reaction proceeds independently of the copper ion and leads to the release of product aldehyde (*11*). The oxidative half-reaction involves the copper ion and molecular oxygen and recycles the reduced enzyme back to its oxidized resting state accompanied by the release of ammonia and hydrogen peroxide. The reduced quinone is a mixture of aminoquinol-$Cu^{2+}$ and semiquinone radical–$Cu^{+}$ couples (Fig. 2A), most (>80%) of the anaerobi-

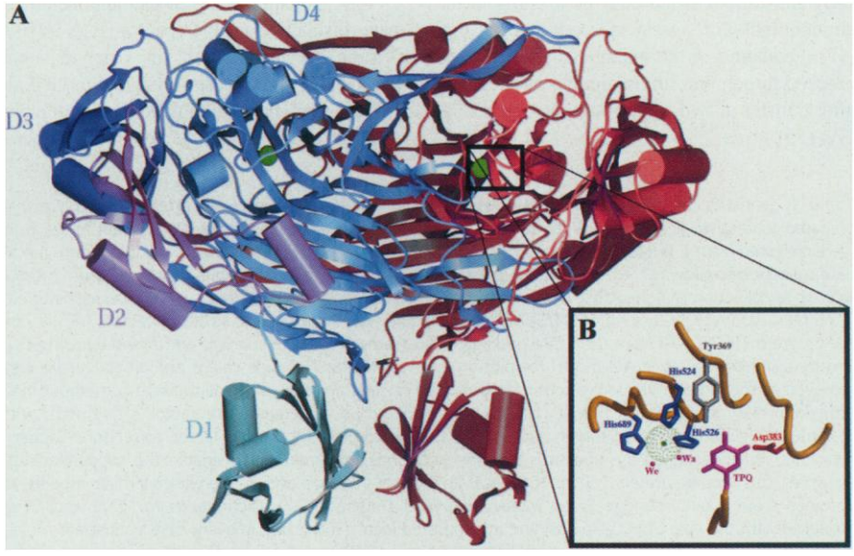


**Fig. 1.** (**A**) Ribbon diagram of ECAO homodimer (*30*). One monomer is colored red and the other is colored by domains (D1, cyan; D2, magenta; D3, royal blue; D4, light blue). Copper ions are shown as green spheres. (**B**) Schematic of ECAO active site, showing the copper ion–ligand geometry and major TPQ conformation (*31*). The water axial and equatorial ligands to the copper ion are labeled Wa and We, respectively. We is mobile and its position is not always fully occupied in CuAO structures.

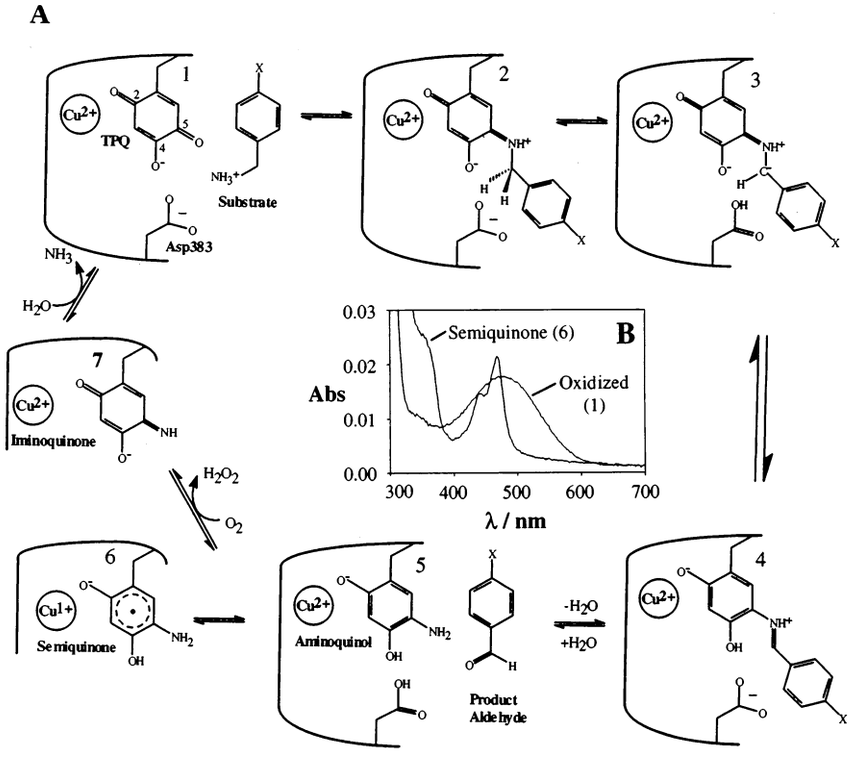


**Fig. 2.** (**A**) Schematic of identified species in the reaction of CuAOs. The enzyme in the oxidized resting state (species 1) reacts with amine substrate to form a substrate Schiff base (species 2). A proton is abstracted by the active-site base ($Asp^{383}$) to form a carbanionic intermediate (species 3) leading to the product Schiff base (species 4). Hydrolysis occurs, releasing the product aldehyde and leaving the reduced cofactor in an equilibrium between aminoquinol-$Cu^{2+}$ (species 5) and semiquinone-$Cu^{+}$ (species 6) coupled states. The reduced cofactor is reoxidized back to TPQ by molecular oxygen, releasing hydrogen peroxide and ammonium ions in the process, and is postulated to do so via an iminoquinone intermediate (species 7) (*10*). (**B**) Typical ECAO solution spectra showing the features in the visible region associated with the oxidized (1) and semiquinone (6) species.

[1]Astbury Centre for Structural Molecular Biology, School of Biochemistry and Molecular Biology, University of Leeds, Leeds LS2 9JT, UK. [2]Department of Biochemistry, Uppsala University, S-751 23, Uppsala, Sweden.

cally substrate-reduced enzyme existing in the aminoquinol-$Cu^{2+}$ state at room temperature (*12*). Oxidation of the quinone is postulated to proceed through an iminoquinone intermediate after transfer of two electrons to dioxygen (Fig. 2A) (*10*).

The oxidation states of the quinone cofactor have distinctive visible spectra (Fig. 2B) (*13*). Visible spectroscopy of the reaction running aerobically in the crystal was used to help identify the maximal accumulation of intermediates (*14*). In addition, the visible spectra of aerobically prepared and anaerobically substrate-reduced ECAO crystals were measured to confirm that the state of the quinone cofactor remained the same both before and after x-ray data collection. We determined structures representing three intermediates in the regeneration of TPQ cofactor by molecular oxygen during catalytic turnover (Table 1).

To investigate the starting point for the oxidative half-reaction, we determined the structure of the anaerobically β-phenylethylamine–reduced ECAO crystallographically to 2.4 Å, which revealed the aminoquinol form of reduced TPQ found in CuAOs (species 5 in Fig. 2A). The aminoquinol is ordered and adopts the dominant conformation of the native oxidized enzyme (Fig. 3A). The Wa ligand on the copper ion is present and is hydrogen-bonded to O-2 of aminoquinol, but the We position of the resting enzyme is vacant (Fig. 4A). The product, phe-

**Table 1.** Statistics for data collection and refinement of models. Native ECAO protein and crystals were prepared as detailed previously (*4*). Intermediates were prepared as described (*21*). X-ray data for each form were collected from a single crystal at 100 K, and the crystals were transferred back into liquid nitrogen after data collection to allow for remeasuring the crystal spectra. In each case, the single-crystal spectrum measured after data collection matched that of the crystal just after preparation. The data were processed with either DENZO/SCALEPACK (*22*) or MOSFLM/SCALA (*23, 24*), and were converted to structure factors ($|F_o|$) by using the program TRUNCATE from the CCP4 package of programs (*24*). Modeling was performed by using O (*25*) and by using the native ECAO model (resolution 2.0 Å) with the TPQ side chains and all active-site waters removed as the initial model. All electron density map calculations and refinements were carried out in CNS (*26*), in cycles of positional Powell minimization and individual temperature factor refinement, with a maximum likelihood function target and an overall anisotropic temperature factor correction. Copper ion restraints were weakened by adjustment of the nonbonded parameters, to enable the copper ion–ligand distances to more accurately reflect the data. Phenylacetaldehyde and β-phenylethylamine models were obtained from the Cambridge Small Molecule Crystal Database (*27*). Dictionaries for CNS and O were produced with the help of HIC-Up (*28*) and incorporated ideal geometries. In every case a substrate molecule was found located at a crystal contact (involving a D1 and a D2) as well as a surface-bound glycerol molecule. An additional glycerol molecule was located in the solvent-filled intersubunit cavity. Refinements were ceased when the largest $F_o - F_c$ peaks appeared to represent noise, and the $R_{free}$ no longer decreased.

| | Anaerobically substrate reduced | Anaerobically substrate reduced + NO | Aerobically trapped equilibrium species |
|---|---|---|---|
| *Data collection statistics** | | | |
| Beamline | Daresbury SRS, 9.6† | ESRF BM14‡ | Daresbury SRS, 9.5§ |
| Wavelength (Å) | 0.87 | 1.03 | 0.9 |
| Data processing | MOSFLM/SCALA | DENZO/ SCALEPACK | DENZO/ SCALEPACK |
| Resolution (Å) | 2.4 (2.53–2.4) | 2.4 (2.44–2.4) | 2.1 (2.14–2.1) |
| Measured reflections | 304948 | 191118 | 287965 |
| Unique reflections | 69377 | 65769 | 92555 |
| $R_{merge}$‖ | 0.094 (0.336) | 0.074 (0.265) | 0.046 (0.337) |
| $\langle I \rangle / \langle \sigma(I) \rangle$ | 6.0 (2.1) | 16.0 (3.6) | 13.4 (1.8) |
| *Refinement statistics* | | | |
| Completeness (%) | 98.3 (94.7) | 92.5 (92.5) | 88.4 (73.8) |
| Resolution (Å) | 2.4 | 2.4 | 2.1 |
| $R_{work}$ [No. of reflections]# | 0.181 [66738] | 0.181 [63469] | 0.195 [89296] |
| $R_{free}$ [No. of reflections]# | 0.239 [2400] | 0.231 [2274] | 0.239 [3199] |
| rms deviations** | | | |
| Bond (Å) | 0.006 | 0.006 | 0.006 |
| Angle (degs) | 1.49 | 1.50 | 1.49 |
| Average B (Å²) | | | |
| Protein | 31.1 (main chain), 33.7 (side chain) | 39.8 (main chain), 41.4 (side chain) | 28.5 (main chain), 30.6 (side chain) |
| Ligands | 43.0 | 52.8 | 43.2 |
| Solvent | 46.1 | 51.4 | 47.0 |
| RMS of protein-bonded B's (Å²) | | | |
| Main chain | 1.8 | 1.0 | 1.2 |
| Side chain | 3.7 | 2.0 | 2.3 |
| No. of atoms in refined model | | | |
| Protein | 11349 | 11349 | 11349 |
| Solvent | 1480 | 1443 | 1470 |
| Nonprotein/solvent atoms†† | 2 ($Cu^{2+}$), 9 (β-PEA), 18 (PAAld), 4 ($Ca^{2+}$), 12 ($C_3O_3H_8$) | 2 ($Cu^{2+}$), 9 (β-PEA), 18 (PAAld), 4 (NO), 4 ($Ca^{2+}$), 12 ($C_3O_3H_8$) | 2 ($Cu^{2+}$), 9 (β-PEA), 18 (PAAld), 4 ($O_2$), 4 ($Ca^{2+}$), 12 ($C_3O_3H_8$) |

*Numbers in parentheses correspond to those in the last resolution shell. †Data were collected on an ADSC Quantum 4 CCD, oscillation 0.75°. ‡Data were collected on a MAR345 image plate operating in 300 mode, oscillation 1.0°. §Data were collected on a MAR300 image plate operating in 300 mode, oscillation 0.75°. ‖$R_{merge}$ indicates agreement of individual reflections over the set of unique averaged reflections. $R_{merge} = \Sigma_{h,i} |I(h)_i - \langle I(h)_i \rangle| / \Sigma_{h,i} I(h)_i$, where $h$ is the Miller index and $i$ indicates individually observed reflections. #Unweighted crystallographic R value = $\Sigma_h ||F_o(h)| - k|F_c(h)|| / \Sigma_h |F_o(h)|$, where $F_o(h)$ and $F_c(h)$ are the observed and calculated structure factors at Miller index $h$, respectively, and k is a scale factor. **Geometry values of the final protein models as compared with ideal values (*29*). ††β-PEA = β-phenylethylamine; PAAld = phenylacetaldehyde.

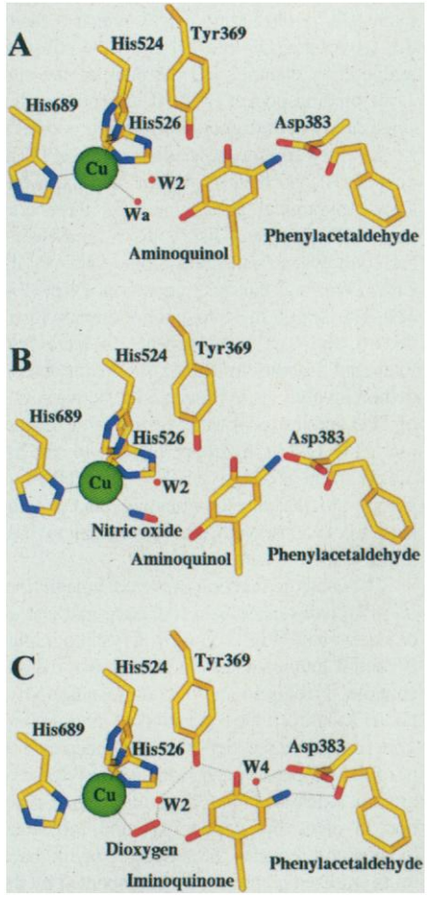


**Fig. 3.** Overview of the essential features of the active sites of the crystal structures (*30*). **(A)** Anaerobic β-phenylethylamine–reduced ECAO. **(B)** Complex of anaerobic β-phenylethylamine–reduced ECAO with nitric oxide. **(C)** Equilibrium turnover species in the crystal by flash-freezing after exposure to β-phenylethylamine, highlighting the proposed mechanistic features of the oxidative half-reaction contained in the structure. Dashed lines indicate key interactions. Red spheres represent mechanistic waters.

nylacetaldehyde, remains bound at the back of the substrate-binding pocket.

To investigate the site of initial dioxygen binding, we determined the complex of β-phenylethylamine–reduced ECAO with the dioxygen mimic nitric oxide, solving it to 2.4 Å resolution. The structure reveals nitric oxide replacing the Wa ligand to the copper ion (Figs. 3B and 4, A and B). Phenylacetaldehyde remains bound at the back of the substrate-binding pocket, and the We ligand site is unoccupied.

The structure of the intermediate formed after prolonged aerobic exposure to excess β-phenyethylamine was trapped by flash-freezing and solved to 2.1 Å resolution (Fig. 3C). The visible spectrum from this crystal matched that of the equilibrium turnover point as assessed by crystal kinetics (*15*). The electron density showed that a dioxygen species replaced the Wa ligand of the copper ion, in a position equivalent to that of bound nitric oxide (Fig. 4C). The We ligand site of the resting enzyme is vacant, and phenylacetaldehyde remains bound at the back of the active site.

All the visible spectra measured from the crystals were bleached, characteristic of either the aminoquinol or the iminoquinone forms of the cofactor. Exposure of the ECAO crystals to β-phenylethylamine in an anaerobic environment caused a change in color from pink (resting enzyme) to yellow (semiquinone) to colorless (aminoquinol) in <10 s. Thus, in the crystal the semiquinone is a transient intermediate, and the cofactor exists as aminoquinol. This contrasts with solution studies, where semiquinone remains evident. The oxidation states of the aminoquinol and iminoquinone differ by two electrons (Fig. 2A). In reduced ECAO, $Cu^{2+}$ could accept one electron, but because there is no acceptor for the second electron, the cofactor is in the aminoquinol state. In contrast, the ligands nitric oxide and dioxygen could accept an electron; therefore, based on the crystal spectra, the electronic form of the cofactor in these intermediates could be either aminoquinol or iminoquinone.

The presence of phenylacetaldehyde in the crystal structures was unexpected, as steady-state kinetics in solution are consistent with the catalytic cycle of CuAOs from several sources operating through a ping-pong mechanism, whereby product aldehyde leaves before dioxygen binds (*16*). The identity of the electron density as product aldehyde rather than substrate amine was confirmed by the presence of a hydrogen bond between the aldehyde group of phenylacetaldehyde and N-5 of cofactor (Fig. 4D). The product aldehyde in the crystal is trapped between domains D3 and D4, which form the substrate entry and product exit channel. In ECAO, the substrate entry channel is restricted in cross section compared with other CuAO structures, and D3 and D4 must move apart to allow access of β-phenylethylamine (*9*). In the crystal, this movement may be restricted by intermolecular contacts. Thus, in crystals of ECAO, the catalytic cycle does not appear to follow a ping-pong mechanism. Although product exit may be less restricted in solution, perhaps in CuAOs with a bulky product, the product may play a role in the oxidative half-reaction (*17*).

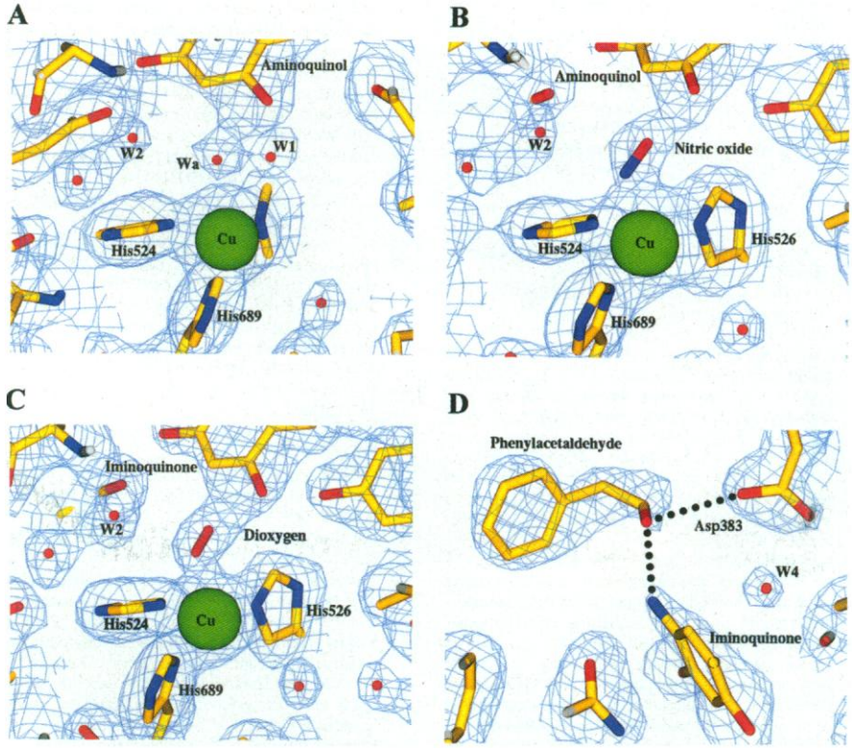


**Fig. 4.** Final $2F_o - F_c$ electron density maps contoured at 1σ (*30*). (**A**) Anaerobic β-phenylethylamine–reduced ECAO. (**B**) Complex of anaerobic β-phenylethylamine–reduced ECAO with nitric oxide. (**C**) Equilibrium turnover species in the crystal by flash-freezing after exposure to β-phenylethylamine. (**D**) Interactions of phenylacetaldehyde in the equilibrium turnover species. Waters (W) are labeled according to their positional equivalence to water positions in the crystal structure of *H. polymorpha* CuAO (*8*). Although the equivalent waters do not always form identical interactions within the two enzymes, their respective positions are mutually exclusive. The orientations of (B) and (C) are identical. (A) has been rotated by ~30° anticlockwise around the vertical compared with (B) and (C), to clearly reveal W1, whose electron density disappears upon binding of a diatomic molecule at the Wa position. The empty We position of the native resting enzyme is located in the plane of the copper histidine ligands between $His^{526}$ and $His^{689}$. Dotted lines represent hydrogen-bonding interactions with position 1 of product aldehyde.

In the nitric oxide complex, the nitric oxide is 2.4 Å from the copper and at an angle of 117°. The crystal structure reveals a hydrogen bond between the oxygen atom of nitric oxide and the O-2 position of cofactor (*18*); this is consistent with the aminoquinol but not the iminoquinone form of the cofactor and could be bound as $Cu^{2+}$-NO–aminoquinol or $Cu^{+}$-$NO^{+}$–aminoquinol. The nonlinear coordination suggests that the major species is $Cu^{2+}$-NO–aminoquinol, with the aminoquinol protonated at O-2. To accommodate the diatomic molecule, the aminoquinol has rotated about χ2 (C1–C4 rotation axis of the ring) by about 20° compared with the substrate-reduced enzyme (Fig. 3, A and B).

The semiquinone-$Cu^{+}$ couple is required for molecular oxygen to bind directly to copper. For bovine serum amine oxidase (BSAO), which has no detectable semiquinone-$Cu^{+}$ couple in anaerobically substrate-reduced enzyme, the rate-limiting step in the oxidative half-reaction is the initial electron transfer to $O_2$, and not $O_2$ binding to the enzyme (*19*). Because electron transfer from $Cu^{+}$ to molecular oxygen would be fast, this suggests that rate-limiting electron transfer to molecular oxygen may be from aminoquinol. The distance between nitric oxide and copper in the crystal is longer than would be expected for a strong bond between copper and nitric oxide (2.4 Å), although the error in this distance may be relatively large. Perhaps molecular oxygen initially binds to the aminoquinol at the O-2 position and the electron transfer from aminoquinol forms superoxide, which would subsequently favor the formation of the $Cu^{2+}$–superoxide ligand interaction.

In the flash-frozen intermediate formed after prolonged aerobic exposure to excess β-phenylethylamine, the dioxygen species occupies the same site as that occupied by

nitric oxide. During the reductive half-reaction, one can postulate that a proton from the amine substrate is transferred by way of the catalytic base to O-4 of the reduced cofactor (*10*). Solution work on BSAO suggests that both protons transferred to the dioxygen in the oxidative half-reaction are derived from the cofactor (*19*). One appears to be the substrate-derived proton at O-4 (*20*), and the other is likely to be transferred from the axial water by way of the O-2 position of cofactor (*10*). In the structure of the equilibrium turnover intermediate of ECAO, proton transfer pathways from both the O-2 and O-4 positions of cofactor are evident.

The O-4 position has a short hydrogen bond (2.4 Å) to the OH of the conserved $Tyr^{369}$ (*9*). Thus, any proton originally at the O-4 posiiton has probably been transferred, leaving O-4 in an ionized state. The OH of $Tyr^{369}$ is linked to the copper-liganded oxygen atom of the dioxygen by a bridging water (W2) that is conserved in all four known structures of CuAOs (Fig. 3C) (*4, 6–8*). Therefore, in the intermediate, the proton from O-4 must either reside on W2 or have been tranferred to the dioxygen. A similar proton transfer route was proposed for BSAO (*19*). Because the proton would probably have completed its transfer, the corresponding second electron transfer to dioxygen would also have occurred. A single electron transfer would yield superoxide and semiquinone. The visible spectrum of the crystal clearly shows that the cofactor is not semiquinone, which suggests that the second electron transfer has also occurred, yielding the iminoquinone and peroxide. The O-2 position is directly hydrogen-bonded to dioxygen (*18*). Because the O-2 position of the iminoquinone is a carbonyl, apparently the O-2 proton has also been transferred to dioxygen. Thus, the observed dioxygen species in this intermediate is probably the product hydrogen peroxide. The two oxygen atoms of dioxygen are 2.8 and 3.0 Å from the copper ion, giving a Cu-O-O angle of 88°. This geometry is consistent with a peroxide character and differs from that observed in the nitric oxide complex. This correlates with the orientation of the cofactor, which is similar to that of native and reduced enzyme and different from the nitric oxide complex (Fig. 3, A and C).

During the oxidative half-reaction, the aminoquinol is oxidized back to TPQ with the release of ammonia and the concomitant reduction of molecular oxygen to hydrogen peroxide. The release of ammonia has been proposed to proceed either by hydrolysis of iminoquinone to leave the enzyme in the resting state or by substrate transimination to form the substrate Schiff base (species 2, Fig. 2A) (*10*). In the equilibrium turnover crystal intermediate of ECAO, a water (W4) is within van der Waals distance (3.0 Å) of C-5 (Fig. 3C), suggesting partial activation for nucleophilic attack. A proton must remain on the base in the active site, $Asp^{383}$, because a hydrogen bond is observed between the acid side chain and the aldehyde group of the phenylacetaldehyde product. Only after the exit of phenylacetaldehyde from the enzyme can $Asp^{383}$ deprotonate, thereby allowing it to accept a proton from the water and fully activating W4 for nucleophilic attack at C-5 to restore the cofactor and release ammonia (step 7 → 1, Fig. 2A). This demonstrates that $Asp^{383}$ has an important catalytic role to play in the oxidative, as well as the reductive, half-reaction. Although a hydrolytic mechanism is clearly indicated in this case, a transimination mechanism (step 7 → 2, Fig. 2A) may be favored at high substrate concentrations or in enzymes from other sources, particularly those with preferences for small aliphatic amines and containing large substrate channels. This work provides a demonstration of the power of cryocrystallography, in conjunction with single-crystal spectrophotometry, in trapping enzyme reaction intermediates and providing detailed mechanistic information about the interaction of oxygen with a metalloenzyme.

## References and Notes


1. J. P. Klinman and D. Mu, *Annu. Rev. Biochem.* **63**, 299 (1994).
2. S. M. Janes *et al.*, *Biochemistry* **31**, 12147 (1992).
3. K. Tanizawa, *J. Biochem.* **118**, 671 (1995).
4. M. R. Parsons *et al.*, *Structure* **3**, 1171 (1995).
5. J. M. Murray *et al.*, *Biochemistry* **38**, 8217 (1999).
6. V. Kumar *et al.*, *Structure* **4**, 943 (1996).
7. M. C. J. Wilce *et al.*, *Biochemistry* **36**, 16116 (1997).
8. R. Li, J. P. Klinman, F. S. Mathews, *Structure* **6**, 293 (1998).
9. C. M. Wilmot *et al.*, *Biochemistry* **36**, 1608 (1997).
10. J. P. Klinman, *Chem. Rev.* **96**, 2541 (1996).
11. A. Rinaldi *et al.*, *Biochem. Biophys. Res. Commun.* **120**, 242 (1984).
12. D. M. Dooley *et al*, *Nature* **349**, 262 (1991).
13. TPQ in the resting enzyme gives it a pink color [M. Mure and J. P. Klinman, *J. Am. Chem. Soc.* **115**, 7117 (1993)], whereas the semiquinone is yellow (*12*) (Fig. 2B). The aminoquinol is essentially colorless, with $\lambda_{max}$ in the UV at 310 nm [C. Hartmann, P. Brzovic, J. P. Klinman, *Biochemistry* **32**, 2234 (1993)]. The iminoquinone has a visible maximum at 454 nm, based on model studies, unless the charge is localized by hydrogen bonds to the O-4 and O-2 positions, whereupon the visible spectrum becomes bleached and a peak appears in the UV with a $\lambda_{max} \sim 350$ nm [M. Mure and J. P. Klinman, *J. Am. Chem. Soc.* **117**, 8707 (1995)].
14. P. A. Williams *et al.*, *Nature* **389**, 406 (1997).
15. An ECAO crystal was mounted within an open quartz capillary embedded in a small Sephadex G25 superfine column filled with stabilizing crystal mother liquor. β-Phenylethylamine solution (100 mM) in crystal mother liquor was pushed over the crystal with use of a syringe pump while visible spectra (integration of twenty 1-s spectra) were recorded continuously in the wavelength range 360 to 600 nm with a microspectrophotometer (4DX Systems AB, Uppsala, Sweden). Spectral changes were observed over 10 min, whereupon an almost featureless equilibrium turnover spectrum was reached, which did not change over the subsequent 50 min of the experiment and was used to define this species.
16. C. E. Taylor, R. S. Taylor, C. Rasmussen, P. F. Knowles, *Biochem. J.* **130**, 713 (1972); U. Nylen and P. Szybek, *Acta Chem. Scand.* **28B**, 1153 (1974); C. Hartmann and J. P. Klinman, *Biochemistry* **30**, 4605 (1991).
17. Inhibition at high substrate concentrations has been observed in solution for pig plasma amine oxidase [K. D. S. Yadav and P. F. Knowles, *Eur. J. Biochem.* **114**, 139 (1981)] and ECAO (P. F. Knowles, unpublished data) and could be a result of slow product aldehyde release.
18. The distances from O-2 of cofactor to the nitric oxide and to the dioxygen molecule are 2.3 and 2.2 Å, respectively. These distances are shorter than expected (normally 2.8 Å) and are probably a result of the greater positional errors associated with positioning a diatomic molecule in the merged electron density between the copper and TPQ at this resolution. The error is largest along the long axis of the diatomic molecule, and thus the cofactor O-2–diatomic distances, which have a linear geometry, have a greater error than the copper-diatomic distances, which have a bent geometry.
19. Q. Su and J. P. Klinman, *Biochemistry* **37**, 12513 (1998).
20. M. Farnum, M. Palcic, J. P. Klinman, *Biochemistry* **25**, 1898 (1986).
21. The aerobic β-phenylethylamine equilibrium turnover intermediate was prepared by transfer of a crystal to 40 μl of 100 mM β-phenylethylamine solution in crystal mother liquor (1.3 M sodium citrate, 100 mM Hepes buffer, pH 7.2). This was then transferred to cryoprotectant (30% glycerol, 1.3 M sodium citrate, 100 mM Hepes buffer, pH 7.2) for 30 s, before being picked up in a loop and flash-frozen in liquid $N_2$ after the turnover in the crystal had reached equilibrium (15 min) (*15*). The anaerobic β-phenylethylamine–reduced crystals were prepared similarly but in an anaerobic glovebox (Belle Technology, Portesham, Dorset, UK) and using degassed solutions. Nitric oxide gas was bubbled into a β-phenylethylamine–reduced crystal drop to give the complex. Anaerobic crystals were flash-frozen while still in the glovebox. Single-crystal visible spectra were then recorded for all the crystals at 100 K in a cold nitrogen stream (Oxford Cryosystems, Oxford, UK) on a microspectrophotometer (4DX Systems AB). The crystals were stored under liquid nitrogen until the synchrotron became available for data collection (between 1 and 4 months).
22. Z. Otwinowski and W. Minor, *Methods Enzymol.* **276**, 307 (1997).
23. A. G. W. Leslie, in *Joint CCP4 and ESF-EACBM Newsletter on Protein Crystallography* (Daresbury Laboratory, Warrington, UK, 1992), vol. 26.
24. Collaborative Computational Project Number 4, *Acta Crystallogr.* **D50**, 760 (1994).
25. T. A. Jones, J. Y. Zou, S. W. Cowan, M. Kjeldgaard, *Acta Crystallogr.* **A47**, 110 (1991).
26. A. T. Brünger *et al.*, *Acta Crystallogr.* **D54**, 905 (1998).
27. Phenylacetaldehyde model: Diphenyl-(2,2-diphenyl-vinyloxy)-acetaldehyde (CSD#66408), H. Preut, R. Stapel, W. P. Neumann, *Acta Crystallogr.* **C43**, 374 (1987). β-Phenylethylamine model: β-Phenylethylamine hydrochloride (CSD#17060), G. Tsoucaris, *Acta Crystallogr.* **14**, 909 (1961).
28. G. J. Kleywegt and T. A. Jones, *Acta Crystallogr.* **D54**, 1119 (1998).
29. R. Engh and R. Huber, *Acta Crystallogr.* **A47**, 392 (1991).
30. SPOCK, written by J. A. Christopher, Centre for Macromolecular Design, Texas A&M University, College Station, TX (1997).
31. T. E. Ferrin, C. C. Huang, L. E. Jarvis, R. Langridge, *J. Mol. Graphics* **6**, 13 (1988).


32. This work was supported by a European Molecular Biology Organisation short-term Fellowship awarded to C.M.W. for work in Uppsala University, a Howard Hughes Medical Institute International Research Scholar award to S.E.V.P., and a grant from the UK Biotechnology and Biological Sciences Research Council. The authors thank M. Halcrow for useful discussions on copper–ligand interactions; J. Murray for useful discussions and help with software; V. Blakeley for preparing the protein; C. Saysell for providing the ECAO solution spectra in Fig. 2B; J. Klinman, D. Dooley, V. Davidson, M. Mure, J. Dove, S. Mills, B. Schwartz, C. Tang, and E. Green for useful discussions at the 1999 "Quinone and Redox Active Amino Acid Cofactors" Gordon Conference; and the staff at the ESRF and Daresbury SRS, particularly L. Duke, G. Leonard, J. Nicholson, and S. Girdwood. The Protein Data Bank accession numbers for the crystal structure coordinates and structure factors are as follows: anaerobically substrate reduced, 1D6U; anaerobically substrate reduced + NO, 1D6Y; and aerobically trapped equilibrium species, 1D6Z.

4 August 1999; accepted 21 October 1999